

A DISPERSION MINIMIZING SCHEME FOR THE 3-D HELMHOLTZ EQUATION WITH APPLICATIONS IN MULTIGRID BASED SOLVERS

CHRISTIAAN C. STOLK

ABSTRACT. We introduce a new, compact stencil discretization of the Helmholtz equation suitable for use in the high-frequency regime with relatively coarse regular meshes. The method, called interpolated optimized finite differences (IOFD), features strongly reduced phase speed errors compared to alternatives in three dimensions, while in two dimensions the method is as good as the best alternative known to us, the quasi-stabilized finite element method. Numerical experiments show that it leads to accurate solutions in constant and smoothly varying media using meshes with five to six points per wavelength and wave propagation over hundreds of wavelengths. Dispersion properties are still good on meshes with down to three points per wavelength, which can be exploited in multigrid based solvers. A priori it is unclear that using coarse meshes, e.g. six points per wavelength, indeed reduces simulation cost, because many solvers have not been tested in this regime. We show that for a modified version of a recently developed hybrid two-grid sweeping solver the cost per degree of freedom changes little, so that these efficiency gains can indeed be obtained. Computation times compare favorably to those of alternatives in the literature.

1. INTRODUCTION

We consider the discretization on regular meshes of the Helmholtz equation

$$(1) \quad -\Delta u - k(x)^2 u = f$$

with large and variable k . These methods are widely used for simulations on unbounded domains, for example in exploration geophysics, using domain sizes, in three dimensions, of up to hundreds of wavelengths [12, 3, 11, 14].

A key issue for such discretizations are the phase speed errors, which are closely related to pollution errors [2]. A second important consideration is solver cost. The discretized Helmholtz operator should of course be cheap to apply and/or invert.

A class of discretizations, that performs relatively well on these criteria, is given by so called compact stencil finite difference methods, that use a 3×3 square or $3 \times 3 \times 3$ cubic stencil in two resp. three dimensions. The corresponding discrete Helmholtz operators can be efficiently applied and inverted compared for example to standard finite difference or finite element methods. Many authors have studied such discretizations and obtained formulae for the coefficients as a function of k and the grid spacing h [2, 7, 8, 10, 4, 17, 15]. While the dispersion behavior varies strongly among the methods, in all cases it can be considered an improvement compared to standard second order differences. In this work we will obtain an improved compact stencil discretization called interpolated optimized finite differences (IOFD), featuring particularly small phase speed errors.

We are interested in two ways of applying the discretized Helmholtz operators. The first is simply as a discretization of (1), where the criterion is that the discrete solutions should approximate the true solutions well. Here we are particularly interested in the use of coarse meshes, say down to five or six points per wavelength, which are for example applied in exploration geophysics [8, 10, 9]. The second application is internally in multigrid based solvers. In a multigrid method, the original mesh is coarsened by a factor two one or more times. On each of the new meshes a discretization of the operator is required. In this application the main criterion for a good discretization is that the multigrid method

converges rapidly. The results concerning the application in multigrid methods are also of interest for recently developed two-grid or multigrid methods with inexact coarse level inverses [3, 14], which are currently some of the fastest solvers in the literature. (The method of [14] will actually be tested here.) Below we will write sometimes the fine level mesh for the original, uncoarsened mesh.

We will now briefly describe our results. The first part of this work focuses on phase speed errors. We will compute phase speed errors for a number of known discretizations in two and three dimensions. Then the IOFD discretization is constructed by first deriving a parameterized family of compact stencil discretizations, and then looking for parameter values that minimize the phase speed errors. *In two dimensions* the resulting phase speed errors are slightly larger than those of the best existing method, the quasi-stabilized finite element method (QS-FEM) [2]. *In three dimensions* there is no generalization of QS-FEM, and we find that the IOFD method has the smallest phase speed errors by a substantial margin. For finite elements, as can be expected, when both the number of points per wavelength and the order is increased, the phase speed errors become very small, smaller than those of compact stencil finite differences, but this comes at considerable cost.

The small phase speed errors for IOFD suggest that accurate solutions are possible even when quite coarse meshes are used, say down to five or six points per wavelength. We will show that this is indeed the case using numerical examples with constant, and smoothly varying velocity models (recall that $k(x) = \frac{\omega}{c(x)}$ with c the medium velocity). In these examples typical phase shift errors are absent even when the waves propagate over several hundred wavelengths. Because of the large domain sizes, we restrict ourselves here to two dimensions.

We then consider the application of the IOFD discretization as coarse level discretization in multigrid based solvers. We will show that in this case IOFD can be used with very coarse meshes with down to three points per wavelength. With such meshes, solutions are generally not accurate enough for direct use, but the approximate solutions can still be used fruitfully in a multigrid method, where they are refined and iteratively improved. This is established using a set of two-dimensional examples, in which a two-grid method with IOFD at both levels converges rapidly (see also the results discussed in the next paragraph). As explained in [15], for the good convergence it is necessary to have very small phase speed errors at these very coarse meshes. The IOFD method (in two and three dimensions) and the QS-FEM method (in two dimensions) are the only discretizations that have this property to our knowledge, and appear to be uniquely suitable for this application.

The results described above show that the IOFD method can be used with coarser meshes than other methods, so that simulation cost can potentially be reduced. However, such a reduction in cost is only obtained if the cost of the solver used to solve the linear systems obtained from the discretization doesn't increase too much with frequency. Whether this occurs is not known for many solvers, at least not below ten points per wavelength. Therefore we will test the behavior of a recently developed three-dimensional fast solver described in [14] in combination with an IOFD discretization at the fine level. The solver uses a two-grid method with an inexact coarse level inverse, given by a double sweep domain decomposition preconditioner. Like described in the previous paragraph, IOFD will also be used as coarse level discretization. Using the SEG-EAGE Salt Model with up to 10^8 degrees of freedom as example, we find that for down to six points per wavelength the cost per degree of freedom changes little when the frequency is increased. Hence there is indeed an efficiency gain associated with the use of coarser meshes, and in this case it is about a factor four when going from ten to six points per wavelength in three dimensions. As a result, computation times of the method are better than those of other methods in the literature.

The setup of this paper is as follows. In section 2 we briefly describe the various discretizations featuring in the paper. In section 3 the computation of phase speed errors is explained, and those of the various existing methods are plotted. In section 4 we introduce our new interpolated optimized finite difference method. Section 5 contains some numerical simulations illustrating the accuracy of the solutions when using the IOFD discretization. Section 6 discusses the use of IOFD in multigrid based solvers. Finally, section 7 contains a brief discussion of some further aspects.

2. SOME DISCRETE HELMHOLTZ OPERATORS

In this section we will describe three types of discretizations of the Helmholtz equation (1), namely standard finite differences, compact stencil finite differences and standard finite elements. In all cases, the degrees of freedom are denoted by $u_{i,j,k}$ (in three dimensions) and associated with a regular mesh with grid spacing h . For finite element methods of order N the cells are of size Nh , and cell boundaries are located at $i, j, k \equiv 0 \pmod{N}$. Occasionally we will use $d = 2$ or 3 to denote the dimension of space.

For standard finite differences we will analyze the phase speed errors in section 3. Therefore we will briefly describe this discretization of the operator $-\Delta - k^2$ for order N , $N = 2, 4, 6, 8$. Each of the one-dimensional second derivatives in the Laplacian $\Delta = \frac{\partial^2}{\partial x_1^2} + \frac{\partial^2}{\partial x_2^2} + \frac{\partial^2}{\partial x_3^2}$ is approximated by a central difference approximation of the given order. These are given by

$$(2) \quad D_2^{(N)} u_i = h^{-2} \sum_{j=-N/2}^{N/2} c_j^{(N)} u_{i+j}$$

where the $c_j^{(N)}$ are as in the following table

	$j = -4$	-3	-2	-1	0	1	2	3	4
$N = 2$				1	-2	1			
4			$-\frac{1}{12}$	$\frac{4}{3}$	$-\frac{5}{2}$	$\frac{4}{3}$	$-\frac{1}{12}$		
6		$\frac{1}{90}$	$-\frac{3}{20}$	$\frac{3}{2}$	$-\frac{49}{18}$	$\frac{3}{2}$	$-\frac{3}{20}$	$\frac{1}{90}$	
8	$-\frac{1}{560}$	$\frac{8}{315}$	$-\frac{1}{5}$	$\frac{8}{5}$	$-\frac{205}{72}$	$\frac{8}{5}$	$-\frac{1}{5}$	$\frac{8}{315}$	$-\frac{1}{560}$

The discrete approximation to the term $-k(x)^2 u$ in (1) is simply given by $-k_{i,j,k}^2 u_{i,j,k}$. The two-dimensional case can be done similarly.

For constant k , compact stencil finite difference discretizations take the form

$$(3) \quad (Au)_{i,j,k} = \sum_{(l,m,n) \in \{-1,0,1\}^3} a_{l,m,n} u_{i+l,j+m,k+n}.$$

Because of symmetry, there are four different coefficients A_j , $j = 0, 1, 2, 3$ and

$$(4) \quad a_{l,m,n} = A_{|l|+|m|+|n|}$$

In 2-D we have

$$(5) \quad (Au)_{i,j} = \sum_{(l,m) \in \{-1,0,1\}^2} a_{l,m} u_{i+l,j+m}.$$

and there are three different coefficients A_j , $j = 0, 1, 2$ and

$$(6) \quad a_{l,m} = A_{|l|+|m|}$$

The choice of coefficients is done in different ways in [2, 7, 8, 10, 4, 17, 15]. The QS-FEM method [2] is a two-dimensional method, for which the coefficients are given modulo an

overall normalization by

$$(7) \quad \begin{aligned} A_0 &= 4 \\ A_1 &= 2 \frac{c_1(\alpha)s_1(\alpha) - c_2(\alpha)s_2(\alpha)}{c_2(\alpha)s_2(\alpha)(c_1(\alpha) + s_1(\alpha)) - c_1(\alpha)s_1(\alpha)(c_2(\alpha) + s_2(\alpha))} \\ A_2 &= \frac{c_2(\alpha) + s_2(\alpha) - c_1(\alpha) - s_1(\alpha)}{c_2(\alpha)s_2(\alpha)(c_1(\alpha) + s_1(\alpha)) - c_1(\alpha)s_1(\alpha)(c_2(\alpha) + s_2(\alpha))} \end{aligned}$$

where $\alpha = kh$ and the auxiliary functions c_1, s_1, c_2, s_2 are defined by

$$(8) \quad \begin{aligned} c_1(\alpha) &= \cos\left(\alpha \cos \frac{\pi}{16}\right) & s_1(\alpha) &= \cos\left(\alpha \sin \frac{\pi}{16}\right) \\ c_2(\alpha) &= \cos\left(\alpha \cos \frac{3\pi}{16}\right) & s_2(\alpha) &= \cos\left(\alpha \sin \frac{3\pi}{16}\right). \end{aligned}$$

We will not discuss the fourth order method of [7] because it contains still a free parameter and one of the authors has later published a sixth order method in [17]. In the latter method variations of k are taken into account. In case of constant k , the coefficients are given in three dimensions by

$$(9) \quad \begin{aligned} A_0 &= +\frac{64}{15} - \frac{14k^2h^2}{15} + \frac{k^4h^4}{20} \\ A_1 &= -\frac{7}{15} + \frac{k^2h^2}{90} & A_2 &= -\frac{1}{10} - \frac{k^2h^2}{90} & A_3 &= -\frac{1}{30} \end{aligned}$$

and in two dimensions by

$$(10) \quad \begin{aligned} A_0 &= \frac{10}{3} - \frac{41k^2h^2}{45} + \frac{k^4h^4}{20} \\ A_1 &= -\frac{1}{6} - \frac{k^2h^2}{90} & A_2 &= -\frac{2}{3} - \frac{k^2h^2}{90}, \end{aligned}$$

again modulo an overall constant.

In [8, 10, 4, 15] the contributions to $-\Delta - k^2$ are split in a contribution from $-\Delta$ and a contribution from $-k^2$. We define a three dimensional mass matrix M depending on three parameters $\alpha_1, \alpha_2, \alpha_3$, which is symmetric and such that the entries of each row add up to one, given by

$$(11) \quad \begin{aligned} (Mu)_{i,j,k} &= \sum_{(l,m,n) \in \{-1,0,1\}^3} m_{l,m,n} u_{i+l,j+m,k+n} \\ m_{l,m,n} &= M_{|l|+|m|+|n|} \end{aligned}$$

where now $M_0 = \alpha_1$, $M_1 = \frac{\alpha_2}{6}$, $M_2 = \frac{\alpha_3}{12}$, $M_3 = \frac{1-\alpha_1-\alpha_2-\alpha_3}{8}$. For constant k the discrete form of the term $-k^2u$ is given by $-k^2(Mu)_{i,j,k}$. Before defining minus the Laplacian we define a two-dimensional mass matrix depending on two additional parameters α_4, α_5

$$(12) \quad \begin{aligned} (N^{[1,2]}u)_{i,j,k} &= \sum_{l,m \in \{-1,0,1\}^2} n_{l,m} u_{i+l,j+m,k} \\ n_{l,m} &= N_{|l|+|m|} \end{aligned}$$

with $N_0 = \alpha_0$, $N_1 = \frac{\alpha_1}{4}$, $N_2 = \frac{1-\alpha_1-\alpha_2}{4}$. Each of the second derivatives in the Helmholtz operator will be discretized using the tensor product of a two-dimensional mass matrix and the standard second order discrete second derivative $D_2^{[j]}$, where $j = 1, 2$ or 3 indicates along which axis the second derivative operators. The resulting matrix is

$$(13) \quad -D_2^{[1]} \otimes N^{[2,3]} - D_2^{[2]} \otimes N^{[1,3]} - D_2^{[3]} \otimes N^{[1,2]} - k^2 M$$

In the two-dimensional case there are in total three parameters $\alpha_1, \alpha_2, \alpha_3$, with $M_0 = \alpha_1$, $M_1 = \frac{\alpha_2}{4}$, $M_2 = \frac{1-\alpha_1-\alpha_2}{4}$, and $N_0 = \alpha_3$, $N_1 = \frac{1-\alpha_3}{2}$.

An advantage of this formulation using tensor products is that in case of PML layers aligned with the coordinate axes, the second order operator $D_2^{[j]}$ can simply be replaced by its PML-modified version.

In this way we have derived a family of second order accurate discretizations. In [8] and [10] the same family of discretizations is considered in two resp. three dimensions (but differently parameterized), and coefficients are chosen such that the maximum phase speed error is minimized, where the maximum is taken over all angles and a range of kh corresponding to at least four points per wavelength. This leads to the choices

$$(14) \quad \begin{aligned} \alpha_1 &= 0.4964958 & \alpha_2 &= 0.4510125 & \alpha_3 &= 0.052487 \\ \alpha_4 &= 0.648355362 & \alpha_5 &= 0.296692332 \end{aligned}$$

for the method of [10] and

$$(15) \quad \alpha_1 = 0.6248 \quad \alpha_2 = 0.37524 \quad \alpha_3 = 0.77305$$

for the method of [8].

In [4] and [15] it is observed that smaller phase speed errors are obtained when the parameters α_j are allowed to vary. In [4] a set of 7 parameters (in three dimensions) is chosen piecewise constant. In [15] the above described set of 5 parameters are chosen as piecewise linear functions of $1/G = \frac{kh}{2\pi}$ (which is one over the number of points per wavelength). In other words, they are obtained by linear interpolation from values of the α_j at certain control nodes. The idea of using interpolation will be explored more in the next section. We note that the piecewise linear strategy yields better phase errors, see Figure 2(c) in [4] and Figure 4 in [15]. However, we also note that the two methods are not quite comparable, since first in [15] the phase velocity differences with a fine scale operator are minimized, not with the exact operator, and secondly in [4] a larger number of parameters is used, namely 7 instead of 5.

For completeness we express the A_j in terms of the α_j . We have in 3-D (modulo an overall constant h^{-2})

$$(16) \quad \begin{aligned} A_0 &= 6\alpha_4 - (kh)^2\alpha_1 & A_2 &= -\frac{1}{2}\alpha_5 + \frac{1}{2}(1 - \alpha_4 - \alpha_5) - (kh)^2\frac{1}{12}\alpha_3 \\ A_1 &= -\alpha_4 + \alpha_5 - (kh)^2\frac{1}{6}\alpha_2 & A_3 &= -\frac{3}{4}(1 - \alpha_4 - \alpha_5) - (kh)^2\frac{1}{8}(1 - \alpha_1 - \alpha_2 - \alpha_3) \end{aligned}$$

and in 2-D

$$(17) \quad A_0 = 4\alpha_3 - (kh)^2\alpha_1 \quad A_1 = 1 - 2\alpha_3 - (kh)^2\frac{1}{4}\alpha_2 \quad A_2 = -1 + \alpha_3 - (kh)^2\frac{1}{4}(1 - \alpha_1 - \alpha_2).$$

Finite elements will be used to numerically compute a reference solution in section 5. Also we will compute their phase speed errors in section 3. For their description we start with the one-dimensional case. In this case the finite element cells are the intervals $((j-1)Nh, jNh)$, $j = 1, 2, \dots$, each containing $N-1$ interior points and two boundary points. The reference cell is $(0, N)$, and shape functions on this reference cell are given by standard Lagrange polynomials, which we will denote by $L_j^{(N)}(x)$, and which are one at $x = j$ and zero at $x = 0, 1, \dots, j-1, j+1, \dots, N-1, N$ and defined to be 0 outside $[0, N]$. Letting $k \in \mathbb{Z}$ and $l \in \{0, 1, \dots, N-1\}$, the one-dimensional trial and test functions are given by

$$(18) \quad \psi_{kN+l}^{(N)}(x) = \begin{cases} L_0^{(N)}(\frac{x}{h} - (k-1)N) + L_N^{(N)}(\frac{x}{h} - kN) & \text{if } l = 0 \\ L_l^{(N)}(\frac{x}{h} - kNh) & \text{otherwise} \end{cases}$$

The two and three-dimensional trial and testfunctions are given by tensor products of the $\psi_j^{(N)}$. The finite element discretization is of course derived from the weak form

$$(19) \quad \Phi(u, v) \stackrel{\text{def}}{=} \int_{\Omega} \sum_{j=1}^d \frac{\partial u}{\partial x_j} \frac{\partial v}{\partial x_j} dx - \int_{\Omega} k^2 uv dx = \int_{\Omega} f v dx.$$

The elements of the matrix in the discretization are given by

$$(20) \quad a_{i,j,k;\tilde{i},\tilde{j},\tilde{k}} = \Phi(\psi_{\tilde{i},\tilde{j},\tilde{k}}, \psi_{i,j,k})$$

The contribution from the term $\int_{\Omega} \sum_{j=1}^d \frac{\partial u}{\partial x_j} \frac{\partial v}{\partial x_j} dx$ can be called the stiffness matrix and the contribution from $\int_{\Omega} k^2 uv dx$ can be called the mass matrix. If k is constant (or cellwise constant), the stiffness and mass matrices can be computed exactly. If k is variable, then only the stiffness matrix can be computed exactly, and for the mass matrix some sort of quadrature must be used. For constant k these computations are standard and easily done using a computer algebra system, and we will not write down the resulting coefficients.

For constant k , the finite difference methods are obviously translationally symmetric, i.e. if we denote by $a_{i,j,k;\tilde{i},\tilde{j},\tilde{k}}$ the matrix elements we have

$$(21) \quad a_{i,j,k;\tilde{i},\tilde{j},\tilde{k}} = a_{i+p,j+q,k+r;\tilde{i}+p,\tilde{j}+q,\tilde{k}+r}$$

For the finite elements there is a symmetry under a subset of translations given by the p, q, r that are multiples of N .

3. PHASE SPEED AND PHASE SLOWNESS ERRORS

In this section we describe the computation of phase speed and phase slowness errors. Phase speed and phase slowness errors are equivalent, we will work mostly with the phase slowness form, but in the text we will often not make the distinction. We will give phase slowness errors as a function of the number of mesh points per wavelength for a number of known discretizations. The method to compute the phase slowness errors will also be used in the construction of the IOFD scheme in the next section.

Phase velocity and phase slowness are properties associated with continuous and discrete Helmholtz operators and their plane wave, resp. Bloch wave solutions. A Helmholtz operator with constant, real coefficient k has plane wave solutions such that

$$(22) \quad (-\Delta - k^2)e^{i\xi \cdot x} = 0.$$

If ω is the frequency, c is the velocity and $k = \frac{\omega}{c}$, then there is a phase velocity associated with this solution given by

$$(23) \quad v_{\text{ph}} = \omega \|\xi\|^{-2} \xi.$$

The phase slowness vector is defined by

$$(24) \quad s_{\text{ph}} = \omega^{-1} \xi$$

For the continuous operator the phase velocities are the vectors of length c .

If A is a discretization of $-\Delta - k^2$ on \mathbb{R}^3 that is invariant under all translations, then we can look for vectors ξ such that

$$(25) \quad u_{i,j,k} = e^{i\xi \cdot x_{i,j,k}}$$

(where $x_{i,j,k} = h(i, j, k)$) in the nullspace of A . The phase velocities and phase slowness vectors are defined similarly as above. By phase slowness errors we will mean the relative errors

$$\delta = |c \|s_{\text{ph}}\| - 1|.$$

The action of an operator of the form (3) on a plane wave is easily seen to be given by

$$(26) \quad A e^{i\xi \cdot x_{i,j,k}} = \sigma_A(\xi) e^{i\xi \cdot x_{i,j,k}}$$

where $\sigma_A(\xi)$ is given by

$$(27) \quad \begin{aligned} \sigma_A(\xi) = & A_0 + 2A_1(\cos(h\xi_1) + \cos(h\xi_2) + \cos(h\xi_3)) + 2A_2(\cos(h(\xi_1 + \xi_2)) + \cos(h(\xi_1 - \xi_2)) \\ & + \cos(h(\xi_1 + \xi_3)) + \cos(h(\xi_1 - \xi_3)) + \cos(h(\xi_2 + \xi_3)) + \cos(h(\xi_2 - \xi_3))) \\ & + 2A_3(\cos(h(\xi_1 + \xi_2 + \xi_3)) + \cos(h(\xi_1 - \xi_2 + \xi_3)) + \cos(h(\xi_1 + \xi_2 - \xi_3)) + \cos(h(\xi_1 - \xi_2 - \xi_3))) \end{aligned}$$

Thus finding the phase velocities or slownesses comes down to determining the zeros of $\sigma_A(\xi)$ as a function of ξ . Assuming that A is a good discretization, these will lie close to the sphere $\|\xi\|^2 = k^2$. Therefore we will parameterize $\xi = p\nu$, with $p \in \mathbb{R}_+$ and $\nu \in S^{d-1}$, with d the dimension, and solve for p , to get the phase slowness associated with the direction given by ν . The standard numerical solver `fsolve` in Matlab has been used, as well as the more accurate version `vpasolve`.

In a periodically repeating setting, which is the case for finite elements with $N \geq 2$, the situation is somewhat more complicated. The symmetry property (21) only holds for p, q, r divisible by N . For such operators we consider the Bloch waves

$$(28) \quad u_{i,j,k} = e^{i\xi \cdot x_{i,j,k}} v_{i,j,k}$$

where $v_{i,j,k}$ is periodic with shifts (pN, qN, rN) , p, q, r integers. For given ξ , the action of an operator A with these symmetries is given by an $N^3 \times N^3$ matrix acting on the $v_{i,j,k}$ (in three dimensions) for $0 \leq i, j, k \leq N-1$. We need to find the vectors ξ for which there is a zero eigenvalue. However not all zero eigenvectors correspond to plane waves with wave vectors ξ , because of the presence of $v_{i,j,k}$. In general $v_{i,j,k}$ can correspond to a linear combination of plane waves with wave vectors given by $(p\frac{2\pi}{Nh}, q\frac{2\pi}{Nh}, r\frac{2\pi}{Nh})$, where p, q, r are integers. Assuming that some ξ corresponds to a simple zero eigenvalue and that $u_{i,j,k}$ is close to a plane wave (which is often the case because the eigenfunctions of the continuous operator are plane waves and the operator A is a good approximation of the continuous operator), these integers p, q, r can be determined modulo N , and the wave vector associated with an element of the zero set of A can be determined.

In the computations we will take a somewhat different approach. We will compute all eigenvalues, and then only consider the one whose eigenvector $v_{i,j,k}$ is most closely correlated with (has the in absolute value largest inner product with) the constant function $\tilde{v}_{i,j,k} = 1$. We will say we have found a phase velocity vector at some ξ if this eigenvalue is zero. For standard finite elements and k, h such that the mesh has more than four points per wavelength this was sufficient.

Phase slowness errors are directionally depend, i.e. they depend on $\nu \in S^{d-1}$ defined above. We compute the maximum over ν for a number of schemes. In two and three dimensions these schemes are the finite element schemes of order 1, 2, 3, 4, 6 and 8, the standard finite difference discretizations of order 2, 4, 6 and 8 and the sixth order compact stencil method of [17]. In the graphs below these results will be indicated by the letter FE1, FE2 etc., FD2, FD4, etc. and CHO6. In two dimensions we also have the QS-FEM method of [2] and the method of Jo, Shin and Suh [8], denoted by JSS. In three dimensions we also have the method of Operto Et Al [10], indicated by OPT4. We have not included results on the method of [4], these are given in Figure 2(c) in that work. By $G = \frac{2\pi}{kh}$ we denote the number of points per wavelength. The phase slowness errors as a function of $1/G$ are plotted in Figure 1 and 2. At the end of section 4 we will briefly discuss these results.

4. AN INTERPOLATED OPTIMIZED FINITE DIFFERENCE SCHEME

In this section we will define our new interpolated optimized finite difference scheme (IOFD). The operator family parameterized by the coefficients α_j and given in (11) (12),

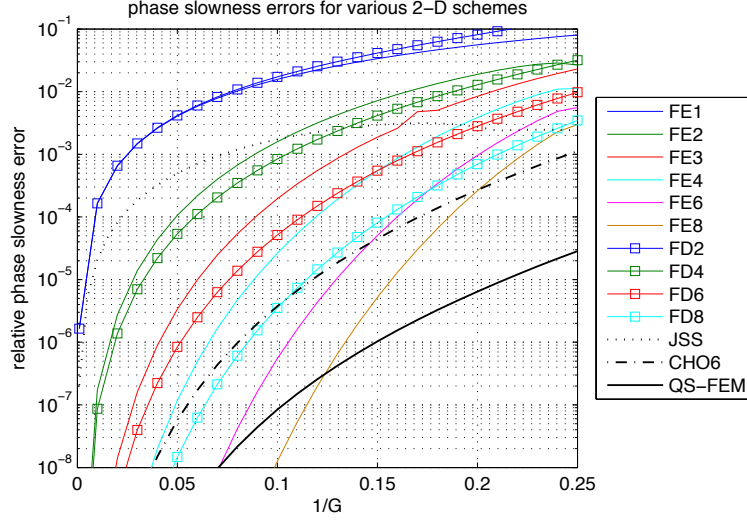


FIGURE 1. Phase slowness errors for some 2-D schemes as a function of the inverse number of points per wavelength $1/G$.

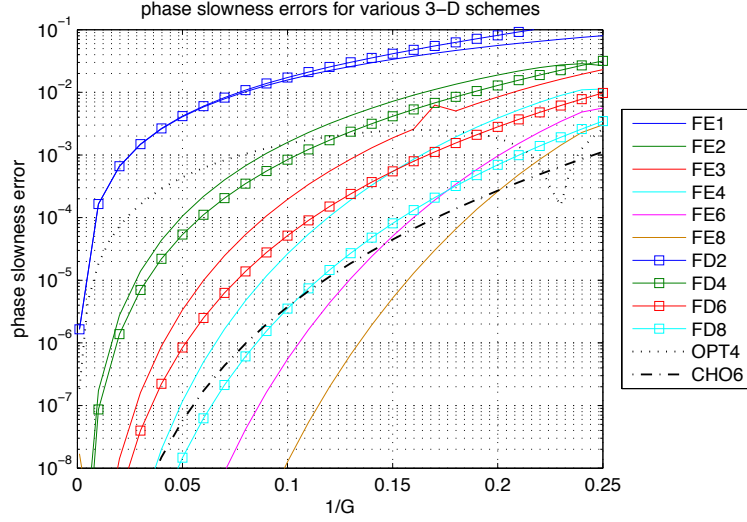


FIGURE 2. Phase slowness errors for some 3-D schemes as a function of the inverse number of points per wavelength $1/G$.

(13) will be used as the starting point. In this work, like in [15] we will let the coefficients α_j depend on $1/G = \frac{kh}{2\pi}$ which equals the inverse number of points per wavelength

$$(29) \quad \alpha_j = \alpha_j(1/G), \quad 1/G = \frac{kh}{2\pi}$$

In this way, clearly a larger family of operators is obtained than when the α_j are constant, so that the resulting phase speed errors can be smaller, see also [4]. Next we will choose a parameterization for these function and we will describe how, by minimizing the phase speed errors in a least-squares sense, we obtain suitable choices of the functions α_j , $j = 1, \dots, 2d - 1$.

In [15] the α_j were chosen to depend piecewise linearly on $1/G$. Here we let α_j depend piecewise polynomially on $1/G$, using Hermite interpolation. We will specify a number of control nodes, and at each node the value of α_j and its first derivative $\frac{\partial \alpha_j}{\partial (1/G)}$ are

prescribed. We will assume that the coefficients α_j vary slowly, so that we can indeed define the four coefficient of the stencil using five parameters depending on $1/G$. If n_C denotes the number of control nodes, in this way the functions α_j are parameterized by $2n_C$ parameters. In total we have $(4d - 2)n_C$ parameters, collectively denoted by P .

Next we specify the objective functional. Denoting by $\delta(\nu, 1/G, P)$ the slowness error as a function of the indicated parameters, this function is given by a discrete approximation of the integral

$$(30) \quad T(P) = \int_0^{G_{\max}} \int_{S^{d-1}} |\delta(\nu, P)|^2 d\nu d(1/G).$$

By n_A we denote the number of angles to discretize the integration over the sphere and by n_G the number of choices for the parameter $1/G$. In two dimensions we chose $n_A = 20$, in three dimensions $n_A = 200$. The $1/G$ axis was discretized in steps of 0.01 in the integral (30).

The objective functional was minimized using the Matlab function `lsqnonlin`, aimed particularly at least-squares problems. We found that the optimization problem using the least squares objective functional converges better than other types of objective functionals, such as a sup-norm. To enforce that the parameters α_j indeed vary slowly a small regularization term was added. For this term we took the sum of the squares of the differences of the subsequent control values for the function values (i.e. not for the derivatives used in the Hermite interpolation).

The results of the optimization for the two- and three-dimensional case are given in Tables 1 and 2. The phase slowness errors as a function of $1/G$ (maximum over angle) are given in Figure 3, together with those of the IOFD and CHO6 methods. Control nodes were chosen in the interval $[0, 0.4]$ with distance 0.05 apart. Slightly better results in three dimensions were obtained if a few extra control nodes were added near zero. For small values of G , around $1/G \lesssim 0.1$, the phase speed errors were very small, and the result started to depend somewhat on the choice of initial values and regularization parameters. These differences were irrelevant, however, since the phase speed errors were always very small, around $\lesssim 10^{-7}$. For values of $1/G \gtrsim 0.1$, resulting stencil coefficients were essentially independent of these details.

The following conclusions can be drawn from the data in Figures 1, 2 and 3. First the QS-FEM method of [2] (in two dimensions) and the IOFD method developed here (in two and three dimensions) perform remarkably well considering their small stencils. They provides a substantial improvement, roughly a factor 25 to 30, in phase errors compared to the compact sixth order scheme CHO6 of [17], which in turn is better than other alternatives. For higher order FD and FE methods, as can be expected, the error becomes small if both the number of points per wavelength and the order N become large, however this effect sets in quite late, e.g. at eight points per wavelength and $N = 8$ the relative phase slowness errors of the finite element method are roughly equal to those of QS-FEM and IOFD.

Next we discuss how much accuracy might be needed, and in how far the improvements will make a difference in simulations. Phase speed errors typically lead to phase shift errors in the solution. The size of this phase shift equals

$$(31) \quad \text{phase error} = 2\pi\delta \frac{L}{\lambda}$$

where L is the distance between source and observation point, λ is the wavelength and δ is the phase slowness error associated with the particular angle of propagation. In view of this it is not unreasonable to require at least that $\delta \lesssim 0.01 \frac{\lambda}{L}$. In a regime of wave propagation over several hundreds wavelengths, using a mesh with five points per wavelength, from the methods considered only QS-FEM and IOFD satisfy this. At six points per wavelength the CHO6 method is near this bound while FE8 (which is much

$1/G$	α_1	$\frac{\partial \alpha_1}{\partial(1/G)}$	α_2	$\frac{\partial \alpha_2}{\partial(1/G)}$	α_3	$\frac{\partial \alpha_3}{\partial(1/G)}$
0.00	0.690457	0.108782	0.285770	-0.219394	0.833361	-0.003066
0.05	0.693489	0.013868	0.278037	-0.094242	0.832105	-0.047970
0.10	0.691798	-0.078442	0.276388	0.021035	0.828594	-0.093390
0.15	0.685399	-0.175575	0.280535	0.139309	0.822575	-0.150175
0.20	0.674651	-0.256238	0.289330	0.213914	0.813406	-0.219891
0.25	0.664492	-0.162723	0.292235	-0.075894	0.803248	-0.173237
0.30	0.658743	-0.079357	0.280634	-0.368742	0.798744	0.013056
0.35	0.649567	-0.289126	0.268790	-0.109125	0.799467	0.006063
0.40	0.632408	-0.404639	0.263741	-0.088077	0.802679	0.125676

TABLE 1. Coefficients two-dimensional IOFD

$1/G$	α_1	$\frac{\partial \alpha_1}{\partial(1/G)}$	α_2	$\frac{\partial \alpha_2}{\partial(1/G)}$	α_3	$\frac{\partial \alpha_3}{\partial(1/G)}$	α_4	$\frac{\partial \alpha_4}{\partial(1/G)}$	α_5	$\frac{\partial \alpha_5}{\partial(1/G)}$
0.0000	0.517047	-0.128231	0.333081	0.002857	0.283241	-0.000089	0.694875	-0.032150	0.275886	0.003602
0.0125	0.523738	-0.038278	0.324029	0.014698	0.280697	-0.010244	0.706215	-0.107275	0.254147	0.003752
0.0250	0.530888	0.026484	0.313399	-0.058155	0.279935	-0.015825	0.708390	-0.066629	0.248576	0.016901
0.0500	0.537095	0.039560	0.303340	-0.063072	0.279560	-0.092408	0.708425	-0.094977	0.244634	-0.014794
0.1000	0.542482	0.090854	0.292077	-0.164698	0.278376	-0.146901	0.701350	-0.181811	0.244231	-0.005689
0.1500	0.546494	0.054652	0.280352	-0.260799	0.276818	0.040023	0.690703	-0.239478	0.243554	-0.027007
0.2000	0.549472	0.086849	0.266004	-0.399426	0.277537	0.090829	0.678083	-0.249610	0.241806	-0.063416
0.2500	0.550195	-0.047748	0.251441	-0.225406	0.278403	-0.007111	0.665015	-0.269271	0.238819	-0.060470
0.3000	0.549247	-0.003809	0.235504	-0.389836	0.278536	0.001697	0.653948	-0.162012	0.234406	-0.116501
0.3500	0.540024	-0.340977	0.225416	-0.096558	0.281206	0.188504	0.642841	-0.285104	0.229717	-0.102619
0.4000	0.521570	-0.406300	0.220498	-0.113976	0.287583	0.107225	0.630481	-0.205847	0.225579	-0.066426

TABLE 2. Coefficients three-dimensional IOFD

more expensive) also qualifies. So in these situations the improved phase speed accuracy obtained by using QS-FEM or IOFD can be expected to have some impact in terms of lower cost compared to FE8 and in terms of improved accuracy compared to CHO6 and other compact stencil methods. The latter will be confirmed in the examples in the next section.

5. NUMERICAL EXAMPLES

In this section we present two numerical experiments, first in a constant medium, and then in a smoothly varying medium. We will present two-dimensional examples with large domain sizes on the order of hundreds of wavelengths.

As mentioned, phase speed errors typically lead to phase shift errors in the solutions. Considering wave propagation over 500 wavelengths as an example, it follows from (31) and the surrounding discussion that these phase shifts errors for IOFD should be negligibly small for meshes with five or six points per wavelength, and still quite small for four and three points per wavelength. For other methods these errors should show up much stronger. In our first example we will verify this numerically, assuming a constant velocity model.

To simulate a point source at a given grid point, we will use the associated column of the mass matrix given in (11) (with the α_j as described in the previous section). An unbounded domain is simulated by adding a damping layer around the domain of interest, with a nonzero imaginary contribution to k that quadratically increases from the boundary of the domain of interest. The discrete equation is computed using a Matlab implementation and exported to disk, and the resulting linear systems are solved using the MUMPS parallel direct solver [1] on a few nodes of the Lisa cluster of surfsara (www.surfsara.nl), or, for the

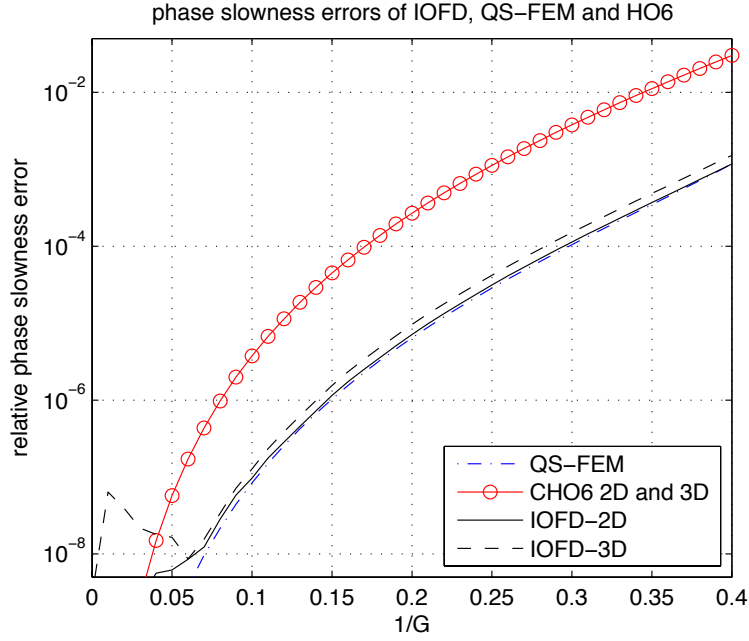


FIGURE 3. Phase slowness errors for the IOFD method compared to QS-FEM and the sixth order method of [17].

smaller cases internally using LU decomposition. In one case (IOFD method at 3 ppw) a sweeping preconditioner was used [13, 14].

To easily observe the absence or presence of the phase shifts, we plot the resulting wave field on a 45 degree part of an annulus, with the radial coordinate varying on an interval of about a wavelength. The location where the real part is minimal, according to the exact solution, is indicated by a line that is plotted. The transformation of the field to polar coordinates is done by using cubic interpolation from the numerical solution on a Cartesian mesh. Schematically this is displayed in Figure 4, where part (b) of the figure is a plot in polar coordinates of the indicated region of part (a).

The results from the computations are displayed in Figure 5. Part (a) shows that for second order finite differences at 10 ppw a clearly visible phase shift already occurs after 20 wavelengths. In (b), (c) and (d) we investigate the sixth order method of [17] at 6, 5 and 4 ppw. In the second case a phase shift is clearly present, while in the third case it becomes rather substantial. In parts (e) to (i) we plot results for the IOFD method at 6, 5, 4, 3 and 2.5 methods. At 3 ppw the phase shift after 500 wavelengths is still moderate, only at 2.5 points per wavelength does it become large and in this case the field is plotted at 100 instead of less than 500 wavelengths from the source.

In our second example k is variable. To avoid that errors due to the discretization of the velocity model become dominant we use a smoothly varying velocity model, namely a smoothed Marmousi model. In this example we will compare a solution with IOFD using a minimum of six points per wavelength with a fourth order finite element solution using twice as many grid points in each direction. In these examples the right hand side was a point source and the linear systems were again solved with MUMPS.

In case of variable coefficients the stencil coefficients will be computed in the following way [14]. We assume the medium coefficient is constant on the grid cells (cubes with grid points as corners). This means that for each grid cell the coefficients A_j , $j = 0, 1, 2, 3$ of equation (4) can be computed. With all the non-zero matrix element one or more grid cells are associated, namely those for which both grid points are a corner point. The

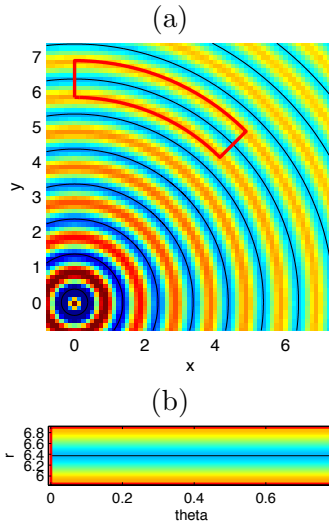


FIGURE 4. Phase shift errors are easily observed by plotting a 45-degree part of an annulus, see figure (b). Cubic spline interpolation is applied to map the data of figure (a) to polar coordinates.

matrix elements for which the coefficient A_0 is used have eight associated grid cells (in three dimensions), when A_1 is used there are four associated grid cells, etc. The coefficient A_j for a certain matrix element are now computed by averaging the coefficients associated with these grid cells. In this way the discretization is somewhat like that of a finite element method. (Indeed in [14] it is argued that this discretization can be viewed as coming from a finite element method with specially chosen test functions.) It results in a symmetric matrix, which is desirable because the operator (1) is symmetric and symmetric systems are cheaper to factorize and solve.

The velocity model is given in Figure 6. It is obtained from the Marmousi model by convolving along both of the axes with a cos square pulse of width 160 meter. We will give results for 50 and 100 Hz. A solution for the first case is given in Figure 7. Figure 8 contains four plots. The top plots are reference amplitudes for obtaining relative errors and the bottom two plots are relative errors with respect to the reference values. In both cases we give results for 50 and for 100 Hz. The reference value is a local average of the absolute value of the solution over a square of about 2 by 2 wavelengths. This is done because the solutions themselves contain nodal points from interfering waves, where the amplitude is very small, and are hence not directly suitable as reference value. Very small relative errors are obtained (except directly at the source point), of about 0.02 to 0.07, the latter occurring in a few spots. The errors could be related to medium inhomogeneities, the location of the errors certainly suggests a correlation.

6. APPLICATION IN MULTIGRID BASED SOLVERS

The last few years there have been several interesting developments in multigrid methods for Helmholtz equations. Different two-grid methods with inexact coarse level solvers have been studied in [3] and [14]. In [3] a number of iterations of shifted Laplacian preconditioned Krylov solver [6] is used as coarse level solver. The method of [14] is based on the multigrid method in [15] with a double sweep domain decomposition preconditioner [13] as coarse level solver. The multigrid method with exact coarse level solver was studied in [15]. There it was shown that the convergence can be strongly improved when phase speed differences between the fine and coarse scale operators are minimized. For this purpose, optimized finite differences were used at the coarse level, and good convergence

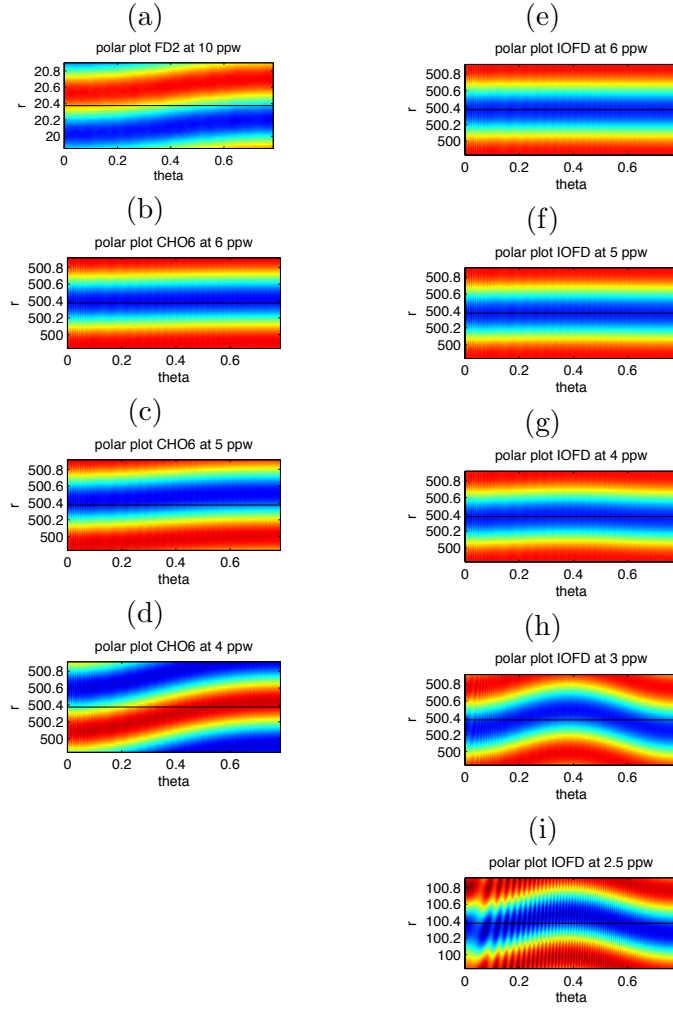


FIGURE 5. Plots of numerical solutions over a 45 degree part of an annulus for several numerical methods. (a) FD2 at 10 ppw; (b), (c), (d) sixth order method of [17] at 6, 5 and 4 ppw;

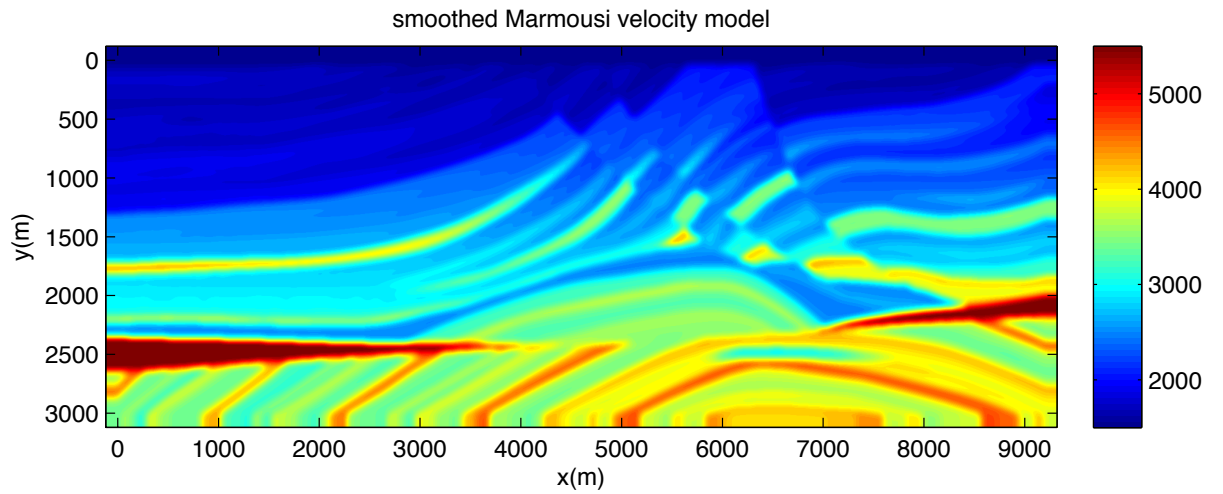


FIGURE 6. Smoothed Marmousi velocity model

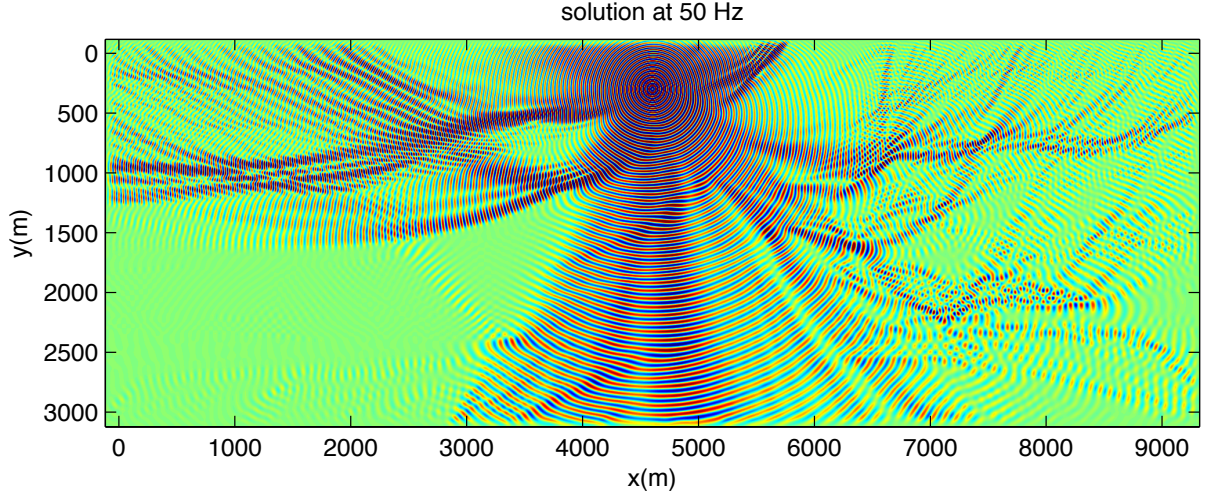


FIGURE 7. Solution from a point source at 50 Hz

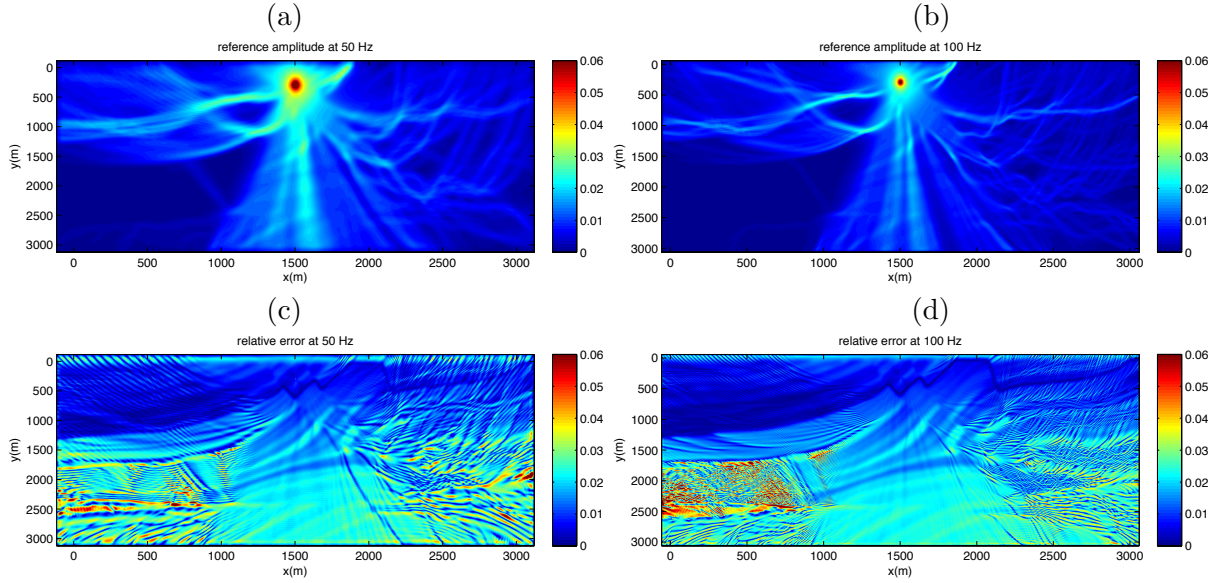


FIGURE 8. Reference values for 50 Hz (a) and for 100 Hz (b). Relative errors in the solutions for 50 Hz (c) and for 100 Hz (d).

was obtained for meshes with down to three points per wavelength at the coarse level. For standard choices of the coarse level discretization it was found that about 10 points per wavelength at the coarse level were needed to have good convergence.

In [15] standard second order finite differences were used as the fine level. Because of the relatively large phase speed errors of this method, the coarse level optimized finite difference method had to be constructed specifically to match the phase speeds of second order finite differences, instead of matching the true phase speed. A better choice is to use method with small phase speed errors at the fine level and at the coarse levels. Here we will use IOFD at all levels.

In the first set of computational results of this section we will show that this results in good convergence of the multigrid method with exact coarse level solver. In a second example we will study the multigrid method with inexact coarse level solver of [14].

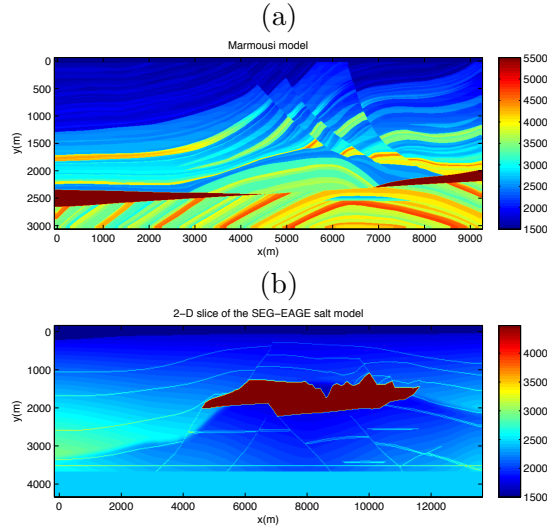


FIGURE 9. Velocity models for the 2-D two-grid experiments. (a) Marmousi (b) 2-D slice of the SEG-EAGE salt model.

In our study of the convergence when using the exact coarse level solver we are again interested in examples with wave propagation over hundreds of wavelengths. Therefore, these experiments are done in two dimensions. For background on multigrid methods, see [16]. Like in [15] most of the components of the multigrid method are standard. Full weighting restriction and prolongation operators are used. As smoother, an ω -Jacobi method is used. We found that $\omega = 0.7$ and $\nu = 4$ (the number of pre- and postsmoothing parameters) are good choices of parameters. In these experiments we used a conventional absorbing boundary layer to simulate an unbounded domain.

We studied the convergence as a function of the number of points per wavelength for three velocity models: A constant model, the Marmousi model and a slice of the 3-D SEG-EAGE salt model. The latter two models are displayed in Figure 9. The parameters of the examples and the observed number of iterations to reduce the residual by 10^6 are given in 3. At down to three points per wavelength the method behaved well. At 2.5 ppw coarse level the method still converged, but the number of iterations increased substantially, and also became more sensitive to the problem size (which was apparent from smaller scale experiments not included in the table).

Note that the application in multigrid methods is quite different from the application as fine level discretization. The method is used at coarser meshes (at three points per wavelength the direct application will in general lead to too large errors). Also, multigrid solvers using IOFD at coarse levels may be developed for other types of fine level discretizations, as long as they use a regular mesh.

We now turn to a multigrid method with an inexact coarse level solver. Such methods are used because in three dimensions it is often too expensive to compute the exact solution. These methods are currently some of the fastest solvers for large problems that are in the literature [3, 14].

Because we are interested in coarse meshes, such as six points per wavelength based on the previous examples, it is *a priori* not clear that the above mentioned solvers perform well. Like many solvers in the literature, they were tested for problems with at least ten mesh points per wavelength. They cannot be assumed to converge as well for larger frequencies, because multigrid convergence depends on frequency, and the same is true for the shifted Laplacian preconditioner [5]. For the double sweep domain decomposition it is

	constant 2400 × 2400		Marmousi 4600 × 750		salt model 2700 × 836	
ppw	freq	its	freq	its	freq	its
5	480	29	150	23	60	18
6	400	8	125	11	50	8
7	342.9	6	107.1	9	42.9	7
8	300	5	93.8	8	37.5	6
9	266.7	5	83.3	7	33.3	6
10	240	4	75	6	30	5

TABLE 3. Iterations required for a two-grid method using IOFD discretization at the fine and coarse level as a function of the number of points per wavelength (ppw)

unclear how the frequency affects the convergence, but a priori it also cannot be assumed to be independent of the frequency.

This raises the question whether we can actually obtain a gain in efficiency by going to coarser meshes. The purpose of the next example is to show that this indeed the case, and to generally show that IOFD can perform well with the solver of [14].

In the following example we will test the method of [14], which is a two-grid method using an inexact coarse level solver given by a double sweep domain decomposition preconditioner (see [13]). The method is modified to use IOFD at both the fine and the coarse levels of the two-grid method. We will take the SEG-EAGE Salt Model as an example, similarly as in [14]. In addition to changing the discretization method we will increase the frequency by a factor $\frac{5}{3}$, so that a minimum of six points per wavelength is used, a regime which has not been tested before for this method. If convergence and cost per degree of freedom would stay constant, there would be an improvement in the cost by a factor of over $(\frac{5}{3})^3 \approx 4.62$ (more than this because cost grows somewhat faster than linear with problem size).

The original SEG-EAGE salt model is of size 13500 x 13500 x 4200 meter, discretized with 20 m grid spacing. We apply the method just described to solve the Helmholtz equation with this velocity model and random or point sources as right hand sides at four different frequencies from 6.25 to 12.5 Hz. Slices of the model are displayed in Figure 10. Parameters in the two-grid method are $\nu = 3$ for the number of pre- and postsmoothing steps and $\omega = 0.65$ in the ω -Jacobi method. Computations were done on the Lisa cluster at surfsara (www.surfsara.nl) using the implementation described in [14]. This system contains 32 parallel nodes with each two intel Xeon processors E5-2650 v2 running at 2.60 GHz and 64 GB memory, connected by Mellanox FDR Infiniband. The use of two intel Xeon units results in 16 cores per node. A maximum of 16 nodes were used in parallel for these computations.

The algorithm is set up to solve for multiple right hand sides simultaneously. In the table of results, the computation time per right hand side is given. In Table 4 some parameters are given, together with the computation time and iteration count to reduce the residual by 10^{-6} . As illustration, plots of a solution are given in Figure 11. It can be observed that the cost increases very little compared to the results of [14], even though frequencies are increased by a factor $5/3$. Some increase in cost can be expected, because the discrete Helmholtz operator using second order finite differences is cheaper to apply than the one using a compact 27-point stencil. Hence reducing the number of points per wavelength in the mesh can indeed lead to corresponding savings in computation time.

As mentioned, the methods of [3] and [14] are some of the fastest currently in the literature. Comparing with these results we see a significant improvement. For example

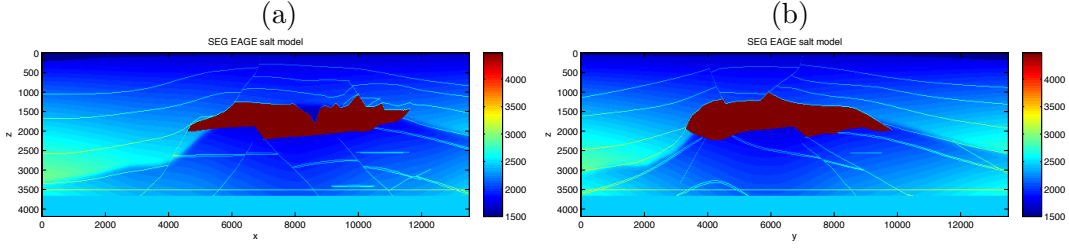


FIGURE 10. SEG-EAGE salt velocity model: (a) (x, z) slice at $y = 6740$ m (b) (y, z) slice at $x = 6740$ m.

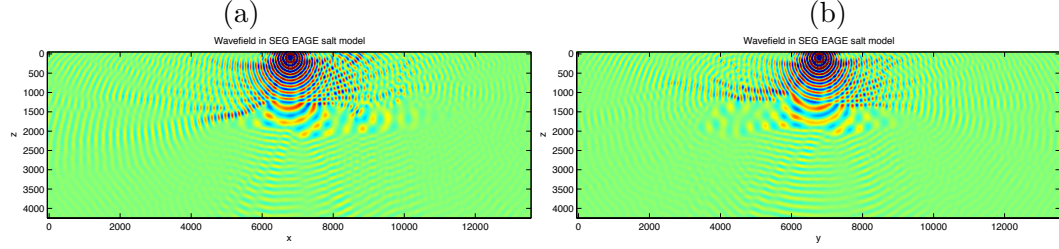


FIGURE 11. Solution to the Helmholtz equation at 12.5 Hz: (a) (x, z) slice at $y = 6740$ m (b) (y, z) slice at $x = 6740$ m.

frequency	6.25	7.87	9.91	12.5
size	338x338x106	426x426x132	536x536x166	676x676x210
# dof	$1.3 \cdot 10^7$	$2.5 \cdot 10^7$	$5.0 \cdot 10^7$	$1.0 \cdot 10^8$
cores	32	64	128	256
# of rhs.	1	2	4	8
iterations	12	12	13	15
computation time/rhs.	26	35	45	73

TABLE 4. Computation times and iteration counts for the SEG-EAGE Salt Model example.

in [3] the SEG-EAGE salt model problem was solved at 10 Hz in 270 seconds on 256 cores of an IBM BG/P machine (with the residual reduced by a factor 10^5 instead of 10^6 in our case). Here we solve the problem at 9.91 Hz using 128 cores in 45 seconds per right hand sides (179 seconds for four right hand sides), a clear improvement¹

7. DISCUSSION

Here we summarize some of the conclusions and further discuss the results.

Using the results the results presented one can make a case for the use of coarse meshes using a minimum of five or six points per wavelength in time harmonic wave simulations. This idea is not new, in the exploration geophysics community it appears to be quite common. However, we found that the methods that have been proposed for this purpose in [8] and [10] can be expected to give substantial phase errors in simulations of large distance wave propagation. By using the new IOFD method (in two or three dimensions) or the QS-FEM method (in two dimensions only), phase errors can be made much smaller.

¹We note that on the other hand the method of [3] uses less memory and has been applied to larger examples than we have shown here.

For the IOFD method we did not study the discretization of medium gradients in detail. The medium was assumed constant on the cells of the mesh as explained in section 5. In the sixth order method of [17] some terms related to medium gradients appear.

When applied in inversion algorithms IOFD and QS-FEM are somewhat more complicated than the methods of [8] and [10], because the operator depends in a more complicated fashion on the coefficients, which means it is more complicated to compute the derivative of the finite difference operator with respect to the medium coefficients. Due to the use of Hermitian interpolation, these derivatives are however continuous for our IOFD method.

Summarizing the results of section 6, we see that the IOFD scheme can be used with meshes with down to three points per wavelength in an application internally in a multigrid method, i.e. an application with remarkably coarse meshes. This was tested with several numerical examples in two dimensions, and also follows from the three-dimensional SEG-EAGE Salt Model example. We tested a multigrid methods with an inexact coarse level solver on a mesh with a minimum of six points per wavelength, because solvers which are tested for ten points per wavelength can in general not be assumed to perform also at these coarser meshes. At six points per wavelength, solver performance was still good, while at five points per wavelength it can be expected that performance degrades. The conclusion is that the use of coarser meshes can indeed lead to faster simulations, but that, depending on the solver, there are limits in how far this is possible. Computation times of this solver using IOFD compared favorably with literature results.

The last conclusion derives from only one example, the SEG-EAGE Salt Model example, and further evidence is desirable. On the other hand there are also other issues with the method of [14], in particular the issue of parallelization of the numerical linear algebra. Therefore we have not studied this further.

REFERENCES

- [1] P. R. Amestoy, I. S. Duff, J. Koster, and J.-Y. L'Excellent. A fully asynchronous multifrontal solver using distributed dynamic scheduling. *SIAM Journal on Matrix Analysis and Applications*, 23(1):15–41, 2001.
- [2] I. Babuška, F. Ihlenburg, E. T. Paik, and S. A. Sauter. A generalized finite element method for solving the Helmholtz equation in two dimensions with minimal pollution. *Comput. Methods Appl. Mech. Engrg.*, 128(3-4):325–359, 1995.
- [3] H. Calandra, S. Gratton, X. Pinel, and X. Vasseur. An improved two-grid preconditioner for the solution of three-dimensional Helmholtz problems in heterogeneous media. *Numer. Linear Algebra Appl.*, 20(4):663–688, 2013.
- [4] Z. Chen, D. Cheng, and T. Wu. A dispersion minimizing finite difference scheme and preconditioned solver for the 3D Helmholtz equation. *Journal of Computational Physics*, 231(24):8152 – 8175, 2012.
- [5] S. Cools and W. Vanroose. Local Fourier analysis of the complex shifted Laplacian preconditioner for Helmholtz problems. *Numer. Linear Algebra Appl.*, 20(4):575–597, 2013.
- [6] Y. A. Erlangga, C. W. Oosterlee, and C. Vuik. A novel multigrid based preconditioner for heterogeneous Helmholtz problems. *SIAM J. Sci. Comput.*, 27(4):1471–1492 (electronic), 2006.
- [7] I. Harari and E. Turkel. Accurate finite difference methods for time-harmonic wave propagation. *J. Comput. Phys.*, 119(2):252–270, 1995.
- [8] Jo, Churl-Hyun and Shin, Changsoo and Suh, Jung Hee. An optimal 9-point, finite-difference, frequency-space, 2-D scalar wave extrapolator. *Geophysics*, 61(2):529–537, 1996.
- [9] H. Knibbe, W. A. Mulder, C. W. Oosterlee, and C. Vuik. Closing the performance gap between an iterative frequency-domain solver and an explicit time-domain scheme for 3D migration on parallel architectures. *GEOPHYSICS*, 79(2):S47–S61, MAR-APR 2014.
- [10] S. Operto, J. Virieux, P. Amestoy, J.-Y. L'Excellent, L. Giraud, and H. B. H. Ali. 3D finite-difference frequency-domain modeling of visco-acoustic wave propagation using a massively parallel direct solver: A feasibility study. *Geophysics*, 72(5, S):SM195–SM211, 2007.
- [11] J. Poulson, B. Engquist, S. Li, and L. Ying. A parallel sweeping preconditioner for heterogeneous 3D Helmholtz equations. *SIAM J. Sci. Comput.*, 35(3):C194–C212, 2013.
- [12] C. D. Riyanti, A. Kononov, Y. A. Erlangga, C. Vuik, C. W. Oosterlee, R.-E. Plessix, and W. A. Mulder. A parallel multigrid-based preconditioner for the 3d heterogeneous high-frequency helmholtz equation.

- Journal of Computational Physics*, 224(1):431 – 448, 2007. Special Issue Dedicated to Professor Piet Wesseling on the occasion of his retirement from Delft University of Technology.
- [13] C. C. Stolk. A rapidly converging domain decomposition method for the Helmholtz equation. *J. Comput. Phys.*, 241:240–252, 2013.
 - [14] C. C. Stolk. A two-grid accelerated sweeping preconditioner for the Helmholtz equation, 2014. [Arxiv.org/abs/1412.0464](https://arxiv.org/abs/1412.0464).
 - [15] C. C. Stolk, M. Ahmed, and S. K. Bhowmik. A multigrid method for the helmholtz equation with optimized coarse grid corrections. *SIAM Journal on Scientific Computing*, 36(6):A2819–A2841, 2014.
 - [16] U. Trottenberg, C. W. Oosterlee, and A. Schüller. *Multigrid*. Academic Press Inc., San Diego, CA, 2001. With contributions by A. Brandt, P. Oswald and K. Stüben.
 - [17] E. Turkel, D. Gordon, R. Gordon, and S. Tsynkov. Compact 2D and 3D sixth order schemes for the Helmholtz equation with variable wave number. *Journal of Computational Physics*, 232(1):272 – 287, 2013.